ISSN 0965-5425, Computational Mathematics and Mathematical Physics, 2021, Vol. 61, No. 10, pp. 1682–1699. © Pleiades Publishing, Ltd., 2021.
Russian Text © The Author(s), 2021, published in Zhurnal Vychislitel'noi Matematiki i Matematicheskoi Fiziki, 2021, Vol. 61, No. 10, pp. 1715–1733.

MATHEMATICAL PHYSICS

Dedicated to Charakhch'yan's scientific advisor Prof. Yu.D. Shmyglevskii

Reflection of Detonation Wave from the Symmetry Plane within a Cylindrical Target for Controlled Thermonuclear Fusion

K. V. Khishchenko[a,*] and A. A. Charakhch'yan[b,]**

[a] *Joint Institute for High Temperatures, Russian Academy of Sciences, Moscow, 125412 Russia*

[b] *Dorodnicyn Computing Center, Federal Research Center "Computer Science and Control," Russian Academy of Sciences, Moscow, 119333 Russia*

**e-mail: konst@ihed.ras.ru*

***e-mail: chara@ccas.ru*

Received February 2, 2021; revised March 14, 2021; accepted June 9, 2021

Abstract—An axisymmetric collision problem for two identical detonation waves traveling towards each other within a preliminary compressed small target consisting of a cylinder filled with fuel consisting of equimolar mixture of deuterium and tritium surrounded by a golden shell and ignited by a proton beam from the cylinder ends is considered. The reflection of the arising nonstationary spatial detonation wave from the symmetry plane is studied. The dependence on time of some characteristics of the flow is discussed. An approximate model of burn that makes it possible to calculate the fuel burn-up factor between the reflected detonation wave and the symmetry plane after the forced termination of the two-dimensional computation due, in particular, to the instability of the fuel–shell interface is developed. The role of two possible mechanisms of the interface instability is studied—its impulse acceleration by the detonation wave (Richtmyer–Meshkov instability) and high-speed fuel sliding along the interface (Kelvin–Helmholtz instability).

Keywords: numerical simulation, controlled thermonuclear fusion, detonation waves, instability of media interface

DOI: 10.1134/S0965542521100055

INTRODUCTION

Modern studies on controlled inertial thermonuclear fusion are mainly devoted to spherical targets because in this direction of research there is hope to obtain the output of thermonuclear energy exceeding the input energy using modern powerful lasers. An attractive feature of cylindrical targets (a cylinder with thermonuclear fuel surrounded by a heavy shell) is the possibility to obtain a nondamping thermonuclear burn wave propagating through cold fuel along the target axis. This allows one, having solved the problem of ignition of a small target that has a low energy gain, increase this factor by increasing the target size along the axis, which requires additional energy for compressing the target but not for its ignition.

Let us discuss works on cylindrical targets in which waves of thermonuclear burn along the axis were considered. In [1], the ignition of the central part of the target was studied, which is modeled by specifying a small high-temperature domain adjacent to the symmetry plane of the problem. In particular, it was shown that an almost stationary nondamping wave can be obtained.

In [2, 3], a preliminary compressed target (in accordance with the fast ignition concept) that is ignited from the end using one or another driver was considered. In [4–6], this was a beam of heavy ions. Almost stationary detonation waves and the so-called radiation waves (see [6]) were obtained; the main propagation mechanism of the radiation waves is heating of cold fuel by high-frequency radiation of hot plasma.

In [7], the igniting driver is a proton beam with heating depth of about ten times lower than that for the beam of heavy ions. It was found that the detonation wave arising after ignition can eventually turn into a near stationary shockless thermonuclear burn wave, the main propagation mechanism of which is nonlocal heating by α-particles created in the fusion reaction between deuterium and tritium nuclei (below it is

are called the DT reaction). Properties of this wave and of its nonstationary precursor generated by high-frequency radiation of hot plasma were studied. No near stationary radiation waves were found in [7].

In the current paper, we consider the interaction of two detonation waves traveling towards each other that simultaneously generated at two opposite ends of the target by identical igniting drivers. The target size is chosen relatively small such that the detonation wave has no time to turn into the shockless wave. The problem symmetry allows us to consider only a half of the target bonded by the symmetry plane. The igniting driver is the same proton beam as in [7].

Earlier, we considered a similar one-dimensional problem (see [8–12]). It was shown that as the detonation wave reflects from the symmetry plane, a wave arises that is well described by the exact solution of the hydrodynamic equations from the known family (see [13]). This solution, which can be easily obtained directly from the hydrodynamic equations, is also used in this paper.

The mathematical model of DT fuel (equimolar deuterium–tritium mixture) is the ordinary model of dense hot plasma. It is based on the equations of one-fluid two-temperature hydrodynamics taking into account the electron and ion heat conduction, radiation (in the diffusive with respect to the solid angle and multigroup with respect to frequency approximation), and fuel plasma heating by the protons of the igniting beam and by α-particles of the DT reaction. The plasma heating by neutrons of the DT reaction is neglected due to a large mean free path.

The main distinction of our model from the models proposed by other researchers is due to the transport of superthermal α-particles. Typically, this is the diffusive approximation of the nonstationary Fokker–Planck kinetic equation in the one-group with respect to the particle velocity (see [4]) or multigroup (see [5]) approximation. It is known (see [14]) that almost entire trajectory of superthermal heavy particles is a straight line. Therefore, it is quite natural to describe the motion of α-particles using the simplified Fokker–Planck equation with the zero diffusive term in the space of velocities (see [15]), for which the particle trajectory is a straight line. In this paper, we use the stationary Fokker–Planck equation.

As in [4–7], we consider a golden shell that is described by the equations of one-temperature hydrodynamics. The shell heating by α-particles, radiation, and heat flux from the fuel is neglected. Note that it was shown in [7, 16] that taking into account the fuel cooling due to the heat flux into the shell increases the ignition energy only by about 10%.

The equation of the fuel state was derived from the semi-empirical equation of the hydrogen state based on the model described in [17]. The gold state is described by the equation described in [18], which ensures the transition to the Fermi gas under strong compression.

We assume that the fuel is preliminary compressed isentropically from the normal state (temperature 4 K, pressure one atmosphere, and density $\rho_a \approx 0.22$ g/cm^3) to the density of $\rho_0 = 1000\rho_a$, which gives the pressure $p_0 \approx 20$ TPa. The shell is assumed to be preliminary compressed isentropically to the pressure p_0, which gives the density of the compressed shell of about 100 g/cm^3.

1. STATEMENT OF THE PROBLEM AND NUMERICAL METHOD

Figure 1 depicts the initial configuration of the fuel and shell in the cylindrical coordinates z, r. The fuel has the shape of a cylinder of radius R and height H. There is an additional region in front of the cylinder for calculating the fuel emitted from the target. Initially, this region is filled with low-density DT gas under atmospheric pressure. The shell has the shape of a cylindrical layer of size ΔR in the coordinate r and H in z.

Figure 1 also shows the types of conditions on different boundaries. On the boundaries of the additional region, except for the symmetry axis, the spatial derivatives of the thermodynamic functions and velocity are assumed to be zero (soft boundary conditions). The soft boundary conditions are also set of the straight boundary AB, which initially coincides with the target end boundary. The external lateral boundary of the shell is a free boundary with atmospheric pressure. On the left boundaries of the shell and the fuel, symmetry boundary conditions are set.

We neglect radiation in the additional region to avoid physically senseless solutions to the radiation diffusion equation in the optically thin case. For the diffusion equation, we assume that there is no external radiation on the line BC. We also neglect the heating of the rarefied DT mixture by the proton beam in the additional region.

During the entire computation time, the boundaries AB and BC are on the given straight line; however, the points B and A may move along this line according to the motion of the interface and the external shell boundary.

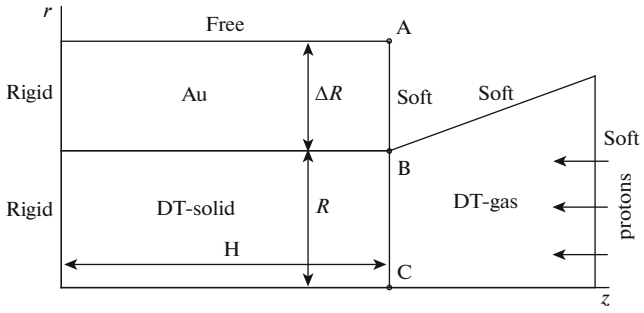

Fig. 1. Target and boundary conditions diagram: "Soft" is the boundary with soft conditions; "Free" is the free boundary; "Rigid" is the symmetry plane.

Soft boundary conditions allow us to exclude from consideration the matter flying out of the boundary. At the same time, such boundaries can reflect the disturbance propagating from the interior thus distorting the solution of the problem. In many problems, the significant distortion of solution can be avoided by choosing an appropriate boundary position and by constructing nonreflective boundary conditions (see [19]). Computations show that the computation procedure described above makes it possible to investigate the target ignition and reflection of the detonation wave from the symmetry plane. Significant distortion of the solution occurs only after the reflected wave leaves the target.

As the igniting driver, we consider a monoenergetic proton beam with the energy of 1 MeV. The intensity J_b of this beam is independent of r for $r \le R$, and it is equal to zero for $r > R$. The function $J_b(t)$ is determined by two parameters: the maximum intensity $J_0 = 10^{19}$ W/cm^2 and the action time of the beam $\Delta t_{pr} = 80$ ps, which, in turn, determines the initial time interval $\Delta t_{0pr} = 0.02\Delta t_{pr}$ during which $J_b(t)$ increases from 0 to J_0:

$$J_b(t) = \begin{cases} J_0 t/\Delta t_{0pr}, & t \le \Delta t_{0pr}, \\ J_0, & \Delta t_{0pr} < t \le \Delta t_{pr}, \\ 0, & t > \Delta t_{pr}. \end{cases} \tag{1}$$

The target geometric parameters are $R = 0.25$ mm (is determined by the proximity condition between the ignition energy and threshold energy), $H = 0.6$ mm, and $\Delta R = 0.2$ mm. The two first parameters correspond to $R\rho_0 \approx 0.55$ g/cm^2 and $H\rho_0 \approx 1.3$ g/cm^2.

As applied to the DT mixture, the hydrodynamic equations take the form

$$\frac{d\rho}{dt} = -\rho\nabla\mathbf{u}, \tag{2}$$

$$\rho\frac{d\mathbf{u}}{dt} = -\nabla p, \tag{3}$$

$$\rho\frac{d\varepsilon_e}{dt} = -p_e\nabla\mathbf{u} - \nabla\mathbf{q}_e + Q_{ei} + D_e + W_e + S, \tag{4}$$

$$\rho\frac{d\varepsilon_i}{dt} = -p_i\nabla\mathbf{u} - \nabla\mathbf{q}_i - Q_{ei} + D_i + W_i, \tag{5}$$

where $d/dt = \partial/\partial t + \mathbf{u}\nabla$ is the Lagrangian time derivative, ρ is the density, $\mathbf{u} = (u_z, u_r)$ is the velocity, p_e and p_i are the electron and ion pressures, $p = p_e + p_i$, ε_e and ε_i are the internal energies of electrons and ions, $\mathbf{q}_e$ and $\mathbf{q}_i$ are the thermal fluxes of electrons and ions, and Q_{ei} determines the exchange of energy between the electrons and ions. The last terms in Eqs. (4) and (5) determine the heating of electrons and ions by the proton beam (D_e and D_i) and by α-particles (W_e and W_i) and the exchange of energy between electrons and radiation (S). The radiation pressure and the transfer of momentum during the slow-down of α-particles are not taken into account in the equation of motion (3).

Equations (2)–(5) are closed by the equations of state for the electronic $p_e(\rho, T_e)$, $\varepsilon_e(\rho, T_e)$ and ionic $p_i(\rho, T_i)$, $\varepsilon_i(\rho, T_i)$ components, where T_e and T_i are the electron and ion temperatures.

We take into account only the primary fusion reaction of deuterium and tritium nuclei as a result of which α-particles with the energy of 3.5 MeV and a neutron are created. The neutrons are assumed to fly out of the fuel without interaction with it. The number of fusion events in unit volume is given by the known formula

$$F = n_{\mathrm{D}} n_{\mathrm{T}} \langle \sigma v \rangle_{\mathrm{DT}} (T_{\mathrm{i}}), \tag{6}$$

where n_{D} and n_{T} are the concentrations of the deuterium and tritium nuclei and $\langle \sigma v \rangle_{\mathrm{DT}} (T_{\mathrm{i}})$ is the reaction rate.

The burn-up of the fuel nuclei is described by the equations

$$\frac{dn_j}{dt} = -n_j \nabla \mathbf{u} - F, \tag{7}$$

where the indices $j = \mathrm{D}$ and T correspond to deuterium and tritium. The additional term in the continuity equation (2) caused by the change of plasma composition due to the DT reaction and the corresponding changes in the equations of state are not taken into account.

The transport of α-particles that are significantly superthermal is described by the stationary kinetic equation in the Fokker–Planck approximation (see [15]) for the distribution function $f(\mathbf{r}, v, \mathbf{\Omega})$, which determines $f(\mathbf{r}, v, \mathbf{\Omega}) dv d\Omega$ as the number of particles in unit volume in the vicinity of the point $\mathbf{r}$ that have the velocity magnitude in the interval dv near v and the direction in the interval $d\Omega$ of the solid angle near $\mathbf{\Omega}$. In addition to the function F, the decelerations of the particle (negative acceleration) on the electrons $a_e(T_e, \rho, v)$ and ions $a_i(T_i, T_e, \rho, v)$, and the particle velocity $v_{\mathrm{th}}(T_i)$ at which it becomes thermal (i.e. at which it stops to be considered as a superthermal particle) are specified. To shorten the notation, we replace the dependence on thermodynamic functions by the dependence on $\mathbf{r}$ assuming that the functions $a_e(\mathbf{r}, v)$, $a_i(\mathbf{r}, v)$, $F(\mathbf{r})$, and $v_{\mathrm{th}}(\mathbf{r})$ are known.

Let all created particles have the same velocity magnitude v_0 and a homogeneous distribution over the solid angle. Then, if the diffusion in the velocity space is ignored in the above inhomogeneous kinetic equation, the latter is reduced to the following Cauchy problem for the homogeneous equation (see [15]):

$$\begin{gathered} v(\mathbf{\Omega}\nabla) f + \frac{\partial a f}{\partial v} = 0, \quad f(\mathbf{r}, v_0, \mathbf{\Omega}) = -\frac{F(\mathbf{r})}{4\pi a(\mathbf{r}, v_0)}, \quad a = a_e + a_i, \\ v_m(\mathbf{r}, \mathbf{\Omega}) = \max(v_{\mathrm{th}}(\mathbf{r}),\, v_b(\mathbf{r}, \mathbf{\Omega})) \le v \le v_0; \end{gathered} \tag{8}$$

here $v_b(\mathbf{r}, \mathbf{\Omega})$ depends on how close the point $\mathbf{r}$ is to the domain boundary along the ray with the direction $-\mathbf{\Omega}$, and it takes into account that particles are not created outside the domain. If $\mathbf{r}$ tends to a point on the domain boundary, then $v_b(\mathbf{r}, \mathbf{\Omega}) \to v_0$ for all $\mathbf{\Omega}$ directed to the interior of the domain. The terms on the right-hand sides of Eqs. (4) and (5) are

$$W_j(\mathbf{r}) = -m_\alpha \int\limits_{(4\pi)} \int\limits_{v_m(\mathbf{r}, \mathbf{\Omega})}^{v_0} f(\mathbf{r}, v, \mathbf{\Omega}) a_j(\mathbf{r}, v) v\, dv\, d\Omega,$$

where $j = e$ or i and m_α is the particle mass.

We use the backward track method (see [20]) to solve problem (8).

The heating of DT plasma by protons is described by their deceleration along the rays $r = \mathrm{const}$ according to the equation

$$v_{\mathrm{p}} \frac{dv_{\mathrm{p}}}{dz} = a_e + a_i,$$

where v_{p} is the proton velocity that decreases from the initial value $v_{0\mathrm{p}}$ to the thermalization velocity v_{th}.

The intensity of the monoenergetic proton beam inside the target is given by the formula $J = n_{\mathrm{p}} v_{\mathrm{p}} m_{\mathrm{p}} v_{\mathrm{p}}^2 / 2$, where n_{p} is the proton concentration, which is assumed to be constant up to their thermalization, and m_{p} is the proton mass. The value n_{p} is determined by the given initial velocity of the pro-

tons v_{0p} and the beam intensity at the target entry (1). The terms on the right-hand sides of Eqs. (4) and (5) are

$$D_e = -\frac{a_e}{a_e + a_i}\frac{\partial J}{\partial z}, \quad D_i = -\frac{a_i}{a_e + a_i}\frac{\partial J}{\partial z}.$$

The plasma radiation is described by an approximation of the stationary transport equation that is diffusive with respect to the solid angle and multigroup with respect to the frequency ν. The multigroup approximation is constructed by partitioning the interval $0 < \nu < \infty$ into N groups $\nu_{l-1} < \nu < \nu_l$, $l = 1, 2, \ldots, N$, $\nu_0 = 0$, $\nu_N = \infty$. In each group, the diffusion equation has the form

$$\nabla \mathbf{q}_l = K_l - \kappa_l^{\mathrm{P}} U_l, \tag{9}$$

where

$$\mathbf{q}_l = -\frac{1}{3\kappa_l^{\mathrm{R}}}\nabla U_l, \quad \kappa_l^{\mathrm{R}} = \frac{\int (\partial B/\partial T_e) d\nu}{\int \kappa^{-1}(\partial B/\partial T_e) d\nu}, \quad \kappa_l^{\mathrm{P}} = \frac{K_l}{\int B d\nu}, \quad K_l = \int \kappa B d\nu,$$

the integration is over the interval $\nu_{l-1} < \nu < \nu_l$, $B(\nu, T_e)$ is the Planck function, and $\kappa = \kappa(\nu, T_e, \rho)$ is the inverse Bremsstrahlung absorption coefficient with regard for the induced radiation. The term on the right-hand side of Eq. (4) is

$$S = -\sum_{l=1}^{N} K_l + \sum_{l=1}^{N} \kappa_l^{\mathrm{P}} U_l,$$

where the first sum determines the plasma cooling and is independent of the partition into groups. We also take into account the cooling of electrons due to inverse Compton effect (see [12]).

The state equations for the two-temperature hydrodynamics and references to the works in which the formulas for the coefficients in the equations above can be found in [7, 12].

The computer code is based on the code for computing axisymmetric flows of plasma and condensed media on moving regular grids consisting of surely convex quadrangles (see [21–26]).

The external boundary of the shell and its boundary with the fuel are computed as Lagrangian grid lines. The difference grid in the main computation fuel domain has $N_r = 40$ intervals on the axis r along the symmetry plane and $N_z = 240$ intervals along the symmetry axis. We also performed test computations with $N_z = 120$. The grid in the shell has 30 intervals on the axis r.

The application of significantly finer grids is restricted by the instability of the interface between the fuel and shell, which manifests itself in the growth of the initially small local boundary disturbance occurring when the detonation wave is formed. For finer grids, the perturbation grows faster, which results in the termination of the computation due to strong curvature of grid cells near the interface.

The number of rays for the solution of problem (8) emitted from each grid cell is $N_{\mathrm{tr}} = 32$. The number of groups for the computation of radiation is $N = 50$, $h\nu_1/k_{\mathrm{B}} = 1.5$ kK, and $h\nu_{N-1}/k_{\mathrm{B}} = 300$ MK. Here h is the Planck constant and k_{B} is the Boltzmann constant.

2. REFLECTION OF DETONATION WAVE

The detonation wave appears at $t \approx 0.15$ ns. Below, we call the symmetry plane $z = 0$ the wall for brevity. Note that, in distinction from detonation due to chemical reactions in gas mixtures, where the detonation wave burns up all the fuel through which it propagates, the thermonuclear reaction continues after reflection.

Figure 2 shows the pressure in the fuel (without the additional region) and in the shell at four successive points in time. The interface between the fuel and the shell, as well as the boundary with the additional region, are shown in bold lines. The arrow points to the local disturbance of the interface, which initially appears when the detonation wave is formed, and then grows due to the boundary instability.

Figure 2a shows the detonation wave of the well-known type (see [27]) with a rarefaction wave adjacent to its front. The time $t = 0.2$ ns corresponds to the position of the detonation wave immediately before its interaction with the wall. The pressure on the wave front increases from the shell to the symmetry axis.

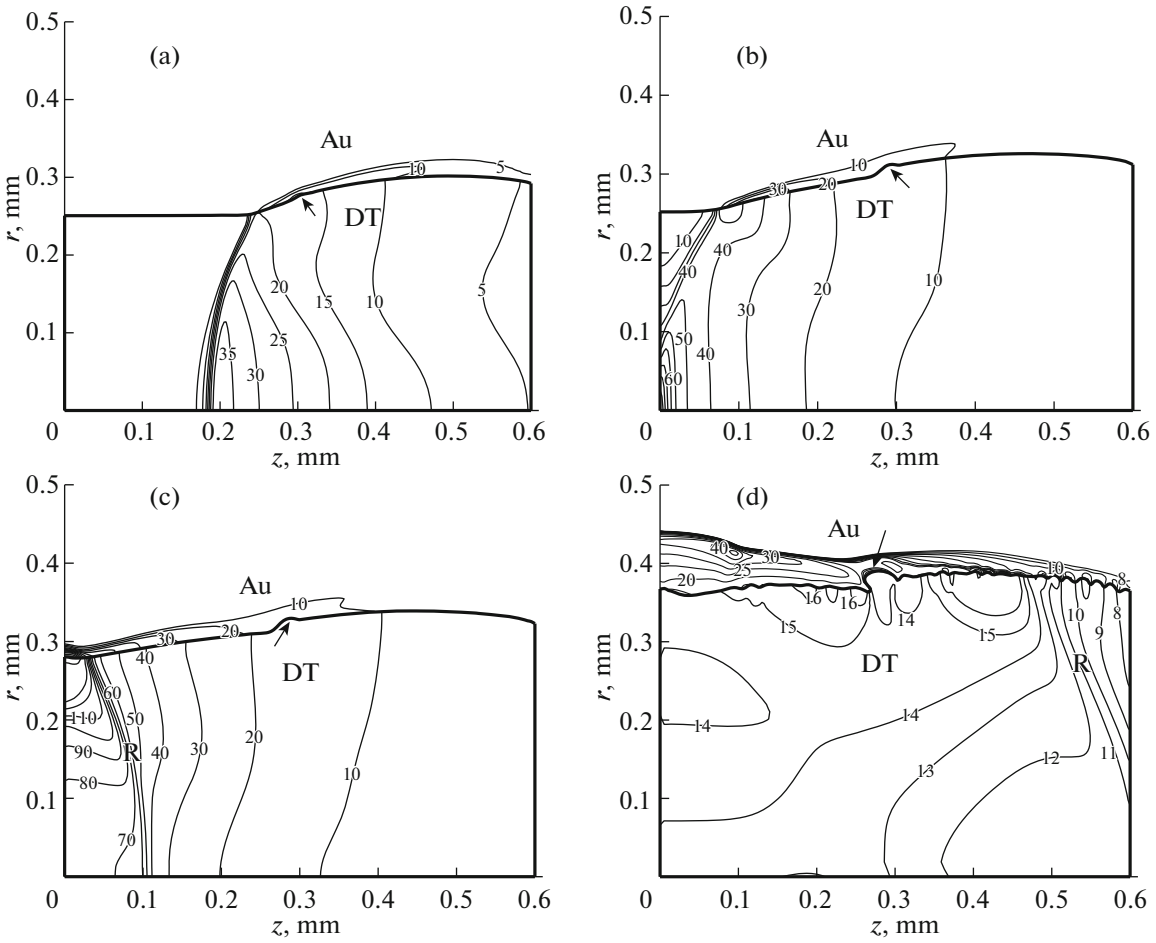

Fig. 2. Isobars (numbers along the curves show pressure in PPa) in the fuel (DT) and shell (Au) at $t = 0.2$ (a), 0.3 (b), 0.35 (c), and 0.5 ns (d); the arrow shows the local disturbance of the boundary; the letter R in (c) and (d) shows the location of the reflected detonation wave.

The wave is not plane: its coordinate z near the symmetry axis is noticeably lower than in the vicinity of the shell. The detonation wave precursor is seen near the symmetry axis.

The initial stage of the detonation wave reflection from the wall is shown in Fig. 2b ($t = 0.3$ ns). Near the boundary with the shell, the wave has not reached the wall yet. The reflection of the other part of the wave gives a high-pressure region in the vicinity of the wall. The further formation of the reflected wave occurs mainly due to the movement of this region along the wall, which will be discussed below in connection with Fig. 3.

Figure 2c shows the reflected detonation wave at $t = 0.35$ ns (the crowding of isolines is marked by the letter R) almost immediately after its formation. Behind the wave front, the pressure near the symmetry axis weakly depends on the spatial coordinates. The high-pressure region is located near the boundary with the shell, having moved here from the vicinity of the symmetry axis (see Fig. 2b). The velocity of the interface has its maximum near the wall.

At the time $t = 0.5$ ns (see Fig. 2d), we see the shock wave in the shell, which detaches from the interface and increases near the wall. In addition to the local disturbance of the interface marked by an arrow, a short-wave disturbance arises on almost entire boundary. In the fuel, the reflected wave has already partly penetrated the additional region.

The pressure behind the reflected wave weakly depends on the spatial variables not only in the vicinity of the symmetry axis but also almost everywhere, except for a small neighborhood of the interface. The similar one-dimensional problem studied in [12] has the same property. The flow between the wall and the reflected wave is well described by the simple solution to the hydrodynamic equations with a linear velocity profile and thermodynamic functions that are independent of the spatial coordinate. The possi-

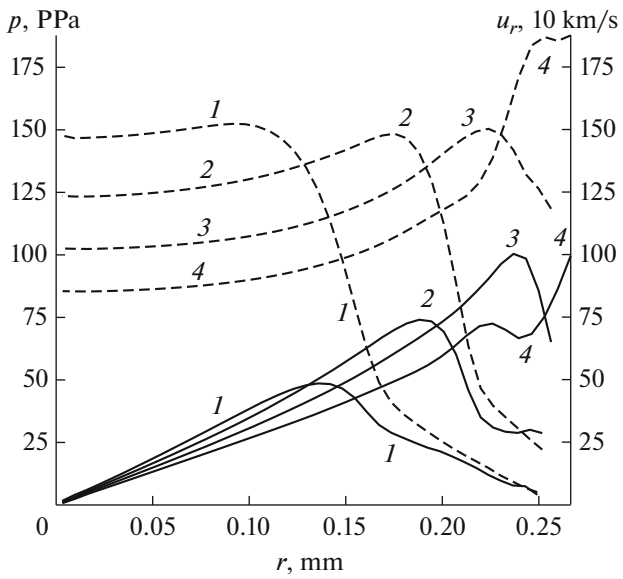

Fig. 3. Pressure (dashed curves) and radial velocity (solid curves) along the wall (symmetry plane) as functions of the radial coordinate at $t = 0.31$ (*1*), 0.32 (*2*), 0.33 (*3*), and 0.34 (*4*) ns.

bility of using this solution for the approximate description of the axisymmetric problem under examination will be discussed in Section 4.

Return to the formation of the reflected detonation wave. Figure 3 shows the profiles of pressure $p(r)$ and radial velocity $u_r(r)$ along the wall at four intermediate time points between $t = 0.3$ ns, when the reflected wave begins to form (Fig. 2b), and $t = 0.35$ ns, when the reflected wave has already formed (Fig. 2c).

It is seen that the high-pressure region generates a high-speed fuel jet along the wall and moves together with the jet in the direction of the shell. The fuel velocity in the jet increases with time and reaches approximately 1000 km/s at $t = 0.33$ ns (see solid line *3* in Fig. 3). The jet blow against the shell gives additional increase of pressure near the shell (see dashed curve *4* in Fig. 3) and creates a shock wave in it stronger than the shock wave formed as the detonation wave moves along the interface. Also, pay attention to the backward wave in the fuel that propagates from the shell to the symmetry axis, which is seen in the last velocity profile with a local minimum (see solid curve *4* in Fig. 3).

The computation on the grid with $N_z = 240$ practically stops at $t \approx 0.5$ ns due to the decrease of the time step, which depends on the stability condition of the explicit scheme for the hydrodynamic equations on strongly curved grids in the vicinity of the curved parts of the interface.

The possibility to perform computations for $t > 0.5$ ns appears if coarser grids are used on which the instability of the interface is not so well defined. However, the accuracy of this computation is significantly lower due to the interaction of the reflected wave with the artificial lateral boundary of the additional computation region. Despite the soft boundary conditions, the matter does not freely fly through this boundary. It seems that another configuration of the additional computation area is required to correctly calculate the escape of the reflected wave from the target.

The absence of the lateral expansion of matter in the additional region is illustrated in Fig. 4 for the computation on the grid with $N_z = 120$ on the time interval from 0.5 to 0.6 ns. Two functions $\overline{F}_{\text{mn}}(t)$ and $\overline{F}_{\text{ad}}(t)$ obtained by averaging the function F (see (6)) over the volume of the main and additional computation domains are shown. It is seen that $\overline{F}_{\text{ad}}(t)$ rapidly increases with time, and at $t = 0.6$ ns it almost coincides with $\overline{F}_{\text{mn}}(t)$, which would be impossible if the fuel were ejected through the lateral boundary of the additional domain.

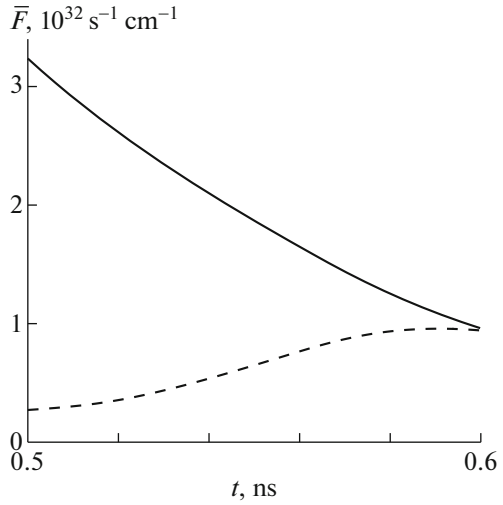

Fig. 4. The generation rate of α-particles F averaged over volume in the main (solid curve) and additional (dashed curve) computation domains on the grid with $N_z = 120$ as functions of time.

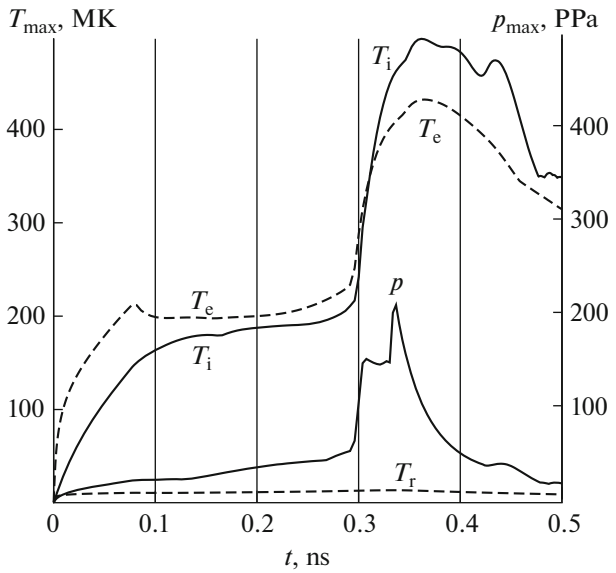

Fig. 5. Maximum (over space) pressure (p) and temperature of ions (T_i), electrons (T_e), and photons (T_r) as functions of time.

3. FLOW CHARACTERISTIC THAT DEPEND ON TIME

Figure 5 shows the maximum thermodynamic parameters (with respect to space)—pressure and temperatures of electrons, ions, and photons—as functions of time. The last temperature is determined by the formula

$$\sum_{l=1}^{N} U_l = \int_0^\infty B(\nu, T_r) d\nu,$$

where U_l is the solution to the diffusion equation (9).

After the formation of the detonation wave and before its reflection from the wall, the maximum pressure point is on the wave front near the symmetry axis. It is seen in Fig. 5 that this pressure increases with time, which indicates that the detonation wave is nonstationary.

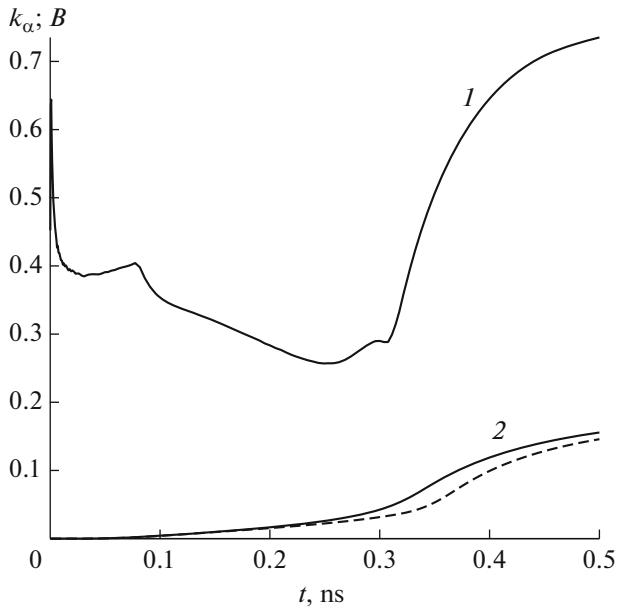

Fig. 6. Relative loss of α-particles power (*1*) and the burn-up factor (*2*) for $N_z = 240$ (solid curve) and 120 (dashed curve) as functions of time.

Before the wave begins to interact with the wall, the electron and ion temperatures reach their maximum values of about 200 MK at a certain distance from the wave. The maximum photon temperature is approximately 20 times lower.

After the detonation wave has reflected from the wall, all the characteristics, except for the photon temperature, increase drastically (the maximum electron and ion temperatures by approximately 2–2.5 times), and then decrease relatively slowly. The first sharp increase in the maximum pressure is due to the blow of the detonation wave against the wall near the symmetry axis (Fig. 2b), and the second peak is a consequence of the blow of the high-velocity jet against the shell near the wall (Fig. 3). The wave reflected from the shell converges to the symmetry axis and gives a small increase in the maximum pressure and ion temperature at $t \approx 0.45$ ns. The stopping of the drop in the maximum pressure and ion temperature at $t \approx 0.5$ ns is a consequence of the interaction of the surrounding fuel with disturbances of the interface (see Fig. 2d).

Figure 6 shows the burn-up factor $B(t)$ (the ratio of the number of DT reaction events to the number of deuterium nuclei in the fuel at $t = 0$) and the relative loss of power of α-particles

$$k_\alpha(t) = 1 - \frac{Y_\alpha(t)}{P_\alpha(t)},$$

where Y_α is the total power of plasma heating by α-particles,

$$Y_\alpha(t) = \int (W_e + W_i) dV,$$

P_α is the total power of the created α-particles,

$$P_\alpha(t) = \frac{m_\alpha v_0^2}{2} \int F(t) dV,$$

W_e and W_i are the terms on the right-hand sides of Eqs. (4) and (5), and F is the number of DT reaction events in unit time in unit volume determined by formula (6); the integration is performed over the fuel volume.

The quantity $k_\alpha P_\alpha$ determines the energy of α-particles thermalizing in the fuel or leaving it in unit time. The energy of α-particles thermalized in unit time is surely small compared with P_α. Even if a particle thermalizes with a temperature of about 500 MK (Fig. 5), which is maximum for the problem under examination, the particle energy is less than 2% of its initial energy. Therefore, we may consider the func-

Table 1. Chosen values of the function $\varphi(t)$ and computed values of the constant C and of the mean density ρ at four time points after the detonation wave reflection

t, ns	φ, μs^{-1}	C, ns	ρ, g/cm^3
0.35	13	–0.27	24
0.4	8	–0.275	13
0.45	6	–0.28	9
0.5	4.75	–0.29	6.9

tion $k_\alpha(t)$ as a fraction of energy of particles that are created in unit time and is carried away by the particles emitted from the fuel. It is seen in Fig. 6 that this fraction is not small.

During the action of the proton beam ($t \le 0.08$ ns), $k_\alpha \approx 0.4$ except for a short initial interval. Then, at $t \approx 0.25$ ns, k_α decreases to about 0.25 and, beginning from $t \approx 0.31$ ns, the function k_α rapidly increases due to the increase in the mean free path of α-particles caused by the decreasing fuel density.

At $t = 0.5$ ns, the burn-up factor $B \approx 0.15$, which is approximately two times less than in the case of the quasi-one-dimensional model considered in [12] with the same initial density and close values of the other parameters ($H = 0.5$ mm and the radius of the cylinder bounding the trajectories of α-particle is 0.1 mm). In the next section, we describe an approximate model of the flow for $t > 0.5$ ns that helps estimate the burn-up factor after the burn stops.

Figure 6 also shows the function $B'(t)$ obtained by the two-dimensional computation on a coarser grid with $N_z = 120$. It is seen that $B'(t) < B(t)$. This enables us to hope that the burn-up factor obtained using a certain grid may be considered as a lower bound on this factor in the exact solution of the problem. Hence, we can investigate targets with large H, which have a greater burn-up factor (see [12]), without increasing the number of grid nodes along the symmetry axis proportionally to H.

4. A ZERO-DIMENSIONAL MODEL OF THE BURN BETWEEN THE WALL AND THE REFLECTED WAVE

The solution of the one-dimensional hydrodynamic equations with a linear velocity profile and spatially constant thermodynamic functions belongs to the known family of solutions described in [13], and it also can be easily obtained from these equations directly [12]. In this solution, the velocity and density are

$$u_z = \varphi(t)z, \quad \varphi(t) = \frac{1}{C+t}, \quad \rho(t) = \rho_0 \frac{C+t_0}{C+t}, \tag{10}$$

where C is an arbitrary constant and $\rho_0 = \rho(t_0)$. It was shown in [12] as applied to the one-dimensional problem similar to the problem considered in this paper that the constant C can be chosen such that the solution to Eq. (10) accurately describes the variation of density in time after the detonation wave is reflected in the region between the wall and the reflected wave.

Figure 7 shows the field of the function u_z/z at four time points after the detonation wave reflection. Table 1 presents the values of the function $\varphi(t)$ from Eq. (10) chosen after a visual analysis of the fields in Fig. 7 as the mean values of the function u_z/z between the wall and the reflected wave. By choosing $\varphi = 13$ at $t = 0.35$ ns (Fig. 7a), we considered the field only near the symmetry axis because in the vicinity of the shell there is a high-pressure region with large gradients of the thermodynamic functions. At three last time points, the function u_z/z varies weakly in almost the entire region between the wall and the reflected wave.

The values of C calculated on the basis of the corresponding values of φ from Eqs. (10) are shown in Table 1. The weak dependence of C on time indicates that Eqs. (10) may be used to approximately describe the dependence of the mean density in the region between the wall and the reflected wave on time.

At the last time $t = 0.5$ ns, almost the entire computation domain is between the wall and the reflected wave. Therefore, we may use the density averaged over the entire volume of the main computation domain as the mean density between the wall and the reflected wave and calculate the mean density at three preceding time points from Eq. (10) with constant C, ρ_0, and t_0 for $t = 0.5$ ns. It is seen in Fig. 8 that the den-

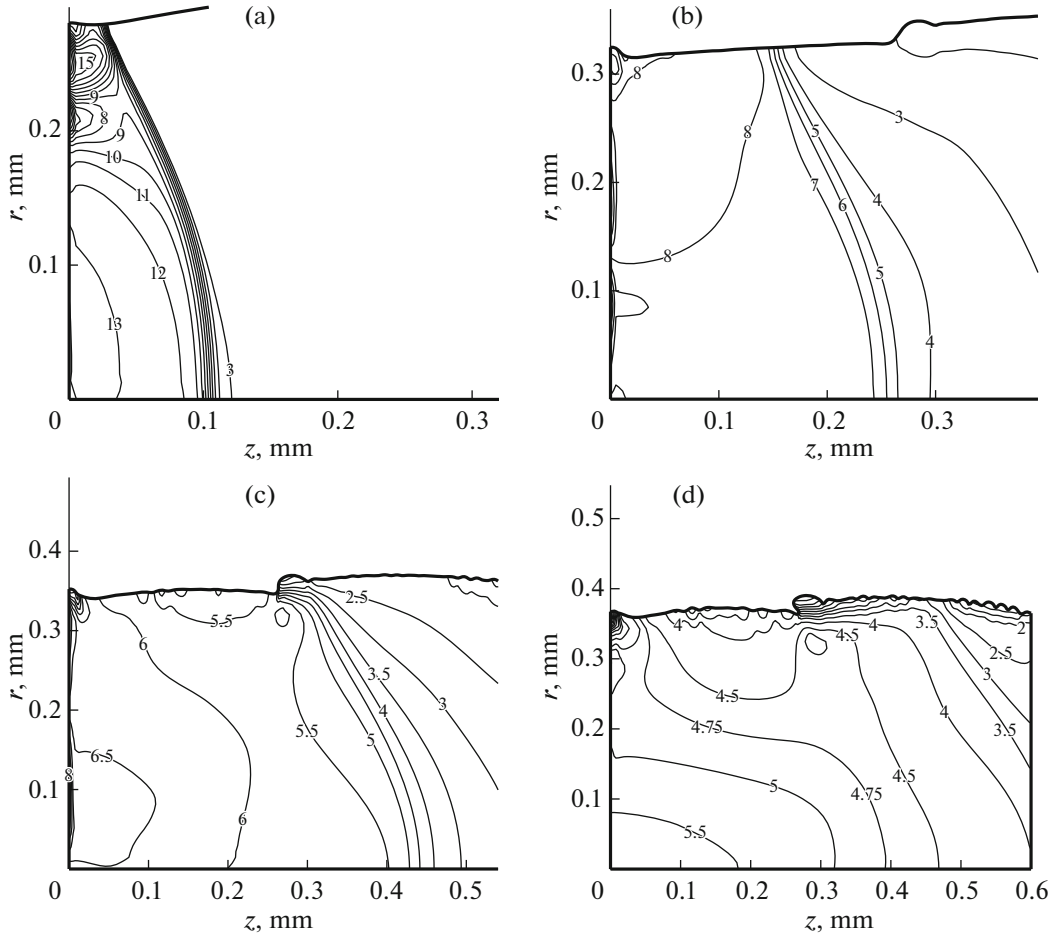

Fig. 7. Isolines of the function u_z/z (μs^{-1}) in fuel after the detonation wave reflection at $t = 0.35$ (a), 0.4 (b), 0.45 (c), and 0.5 (d) ns.

sity at $t = 0.35$ ns (24 g/cm^3) presented in Table 1 gives an adequate approximation of the mean density between the wall and the reflected wave near the symmetry axis.

Let us build a model that approximately describes the time dependence of the thermodynamic functions averaged over the volume of the main computation domain, bearing in mind the possibility of estimating the fuel burn-up factor after the burn stops. Assume that the velocity has only one component u_z with a linear profile in z the slope $\varphi(t)$ of which, along with the density $\rho(t)$, is described by Eqs. (10) with $t_0 = 0.5$ ns. The parameters C and ρ_0 at t_0 are given in Table 1. The plasma is assumed to be one-temperature $T_e = T_i = T$. By substituting Eqs. (6) and (10) into Eq. (7) and setting $n_D = n_T = n$, we obtain the equation

$$\frac{dn}{dt} = -\frac{n}{C+t} - n^2 \langle \sigma v \rangle_{DT}(T),$$

the solution of which satisfies the simple integral equation

$$n(t) = n_0 \frac{C+t_0}{C+t} \exp\left(-\int_{t_0}^{t} n \langle \sigma v \rangle_{DT}(T) dt \right), \tag{11}$$

where $n_0 = \overline{n}_D(t_0)$, and the overline denotes averaging over volume.

The total number of DT reaction events is

$$N_{DT}(t) = N_{DT}(t_0) + V_{mn} \int_{t_0}^{t} F(n,T) dt, \tag{12}$$

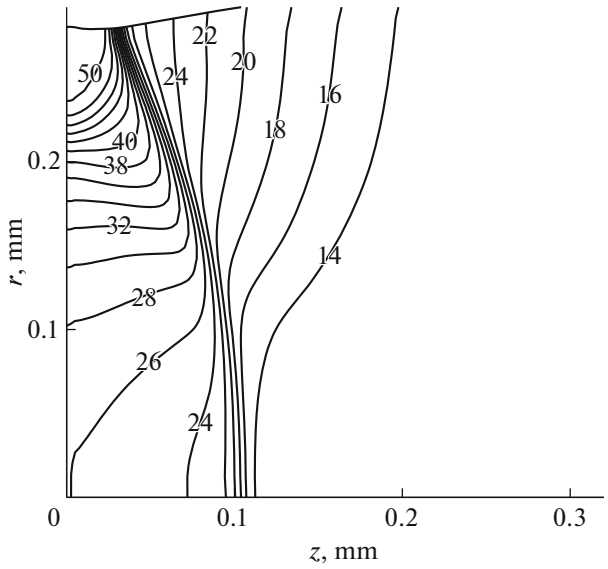

Fig. 8. Isolines of density (g/cm^3) in fuel at $t = 0.35$ ns.

where $N_{\mathrm{DT}}(t_0)$ is determined by the two-dimensional computation, and V_{mn} is the volume of the main computation domain, which is assumed to be independent of time for $t > 0.5$ ns. The temperature $T(t_0) = T_0$ is determined by the condition

$$\bar{F}(t_0) = n_0^2 \langle \sigma v \rangle_{\mathrm{DT}} (T_0),$$

which, due to (12) ensures the equality of derivatives dN_{DT}/dt in the two-dimensional computation and in the approximate model at $t = t_0$.

Equations (10), (11), and (12) should be closed by an equation for the temperature T. If the plasma cooling due to hydrodynamic expansion were significantly greater than for the other cooling or heating mechanisms, then the relation between ρ and T would be defined by the isentrope passing through the point (ρ_0, T_0). Here, this is not the case. Below, for different heating mechanisms, we give the values of the total cooling and heating power, which are the volume integrals of the sum of the corresponding terms on the right-hand sides of Eqs. (4) and (5) obtained by the two-dimensional computation at $t = t_0$ (in units 10^{16} W):

$$Y_{\mathrm{g}} = -\int p(\nabla \mathbf{u}) dV \approx -1.68,$$
$$Y_{\alpha} \approx 1.08, \quad Y_{\mathrm{r}} = \int S dV \approx -0.21,$$
$$Y_{\mathrm{h}} = -\int \nabla(\mathbf{q}_{\mathrm{e}} + \mathbf{q}_{\mathrm{i}}) dV \approx -0.27.$$

The equation for $T(t)$ is taken in the form

$$\frac{dT}{dt} = \left(\frac{dT}{dt}\right)_{\mathrm{g}} \chi,$$

where $(dT/dt)_{\mathrm{g}}$ is the derivative along the isentrope, which is determined by the derivative $d\rho/dt$ in Eq. (10), and $\chi = (Y_{\mathrm{g}} + Y_{\alpha} + Y_{\mathrm{r}} + Y_{\mathrm{h}})/Y_{\mathrm{g}} \approx 0.64$ is the correction coefficient that brings the derivatives dT/dt in line with the results of the two-dimensional computation at $t = t_0$.

The result of the computation of the burn-up factor $B(t)$ for the approximate model is shown in Fig. 9. The burn-up factor increases from 0.15 at $t = 0.5$ ns to approximately 0.18.

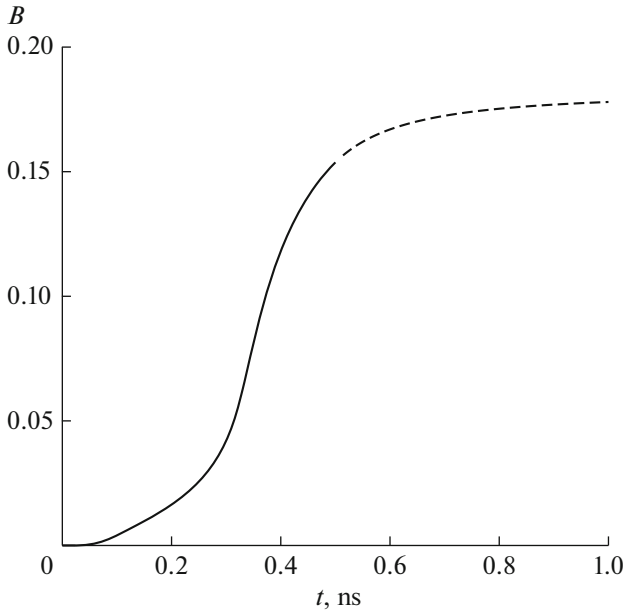

Fig. 9. The burn-up factor as a function of time: two-dimensional computation (solid curve) and the approximate zero-dimensional burn model (dashed line).

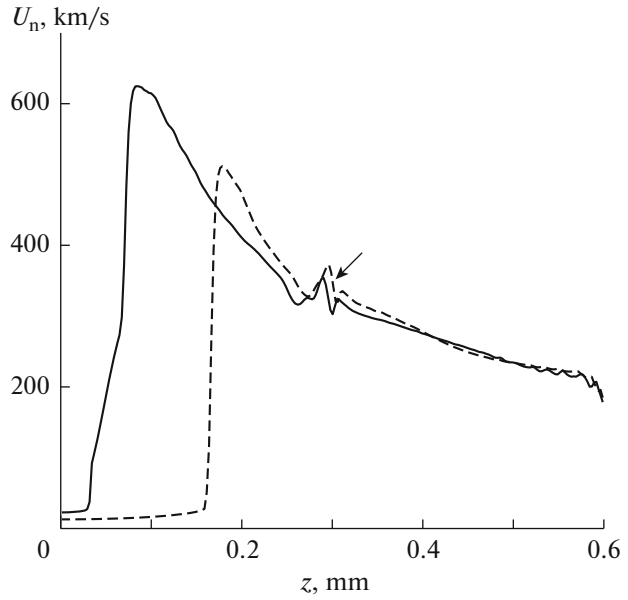

Fig. 10. Normal velocity as a function of z at $t = 0.25$ (dashed curve) and 0.3 (solid curve) ns; the arrow points to the velocity oscillation that causes the local interface disturbance in Fig. 2.

5. INSTABILITY OF THE FUEL–SHELL INTERFACE

Figure 10 shows the normal velocity of the interface U_n depending on z at two points in time when the detonation wave has not yet reached the wall near the interface. The velocity oscillation at $z = z_d \approx 0.3$ mm occurs when the detonation wave is formed, and it causes a local disturbance of the interface in Fig. 2. The acceleration of the interface to the right of the oscillation (for $z > z_d$) is due to fast heating of the fuel by the proton beam. The interface to the left of the oscillation (for $z < z_d$) is accelerated by the detonation wave. The growth of U_n with decreasing z is due to the growth of pressure on the wave front in the course

of its propagation. The comparison of profiles $U_n(z)$ for two time points shows that, after the front has passed, the normal velocity at the fixed interface point decreases with time due to the decrease of pressure behind the detonation wave front.

Note that there are short-wave disturbances of the profile $U_n(z)$ near the extreme point $z = 0.6$ mm, which seems to be a purely computational effect. For two marked time points, these disturbances do not lead to noticeable interface disturbances. However, the occurrence of short-wave interface disturbances that occur later (see Fig. 2d) is most probably caused by the short-wave disturbances of the profile $U_n(z)$ in Fig. 10.

There are two mechanisms of instability development in the problem under consideration. The first mechanism is the Richtmyer–Meshkov (RM) instability caused by the impulse (or close to impulse) interface acceleration that occurs when the detonation wave passes through the fuel and generates a shock wave in the shell. In the case of a plane interface that has the same impulse acceleration at all interface points, the amplitude d of small sinusoidal disturbances with the wave length λ (the initial disturbance amplitude $d_0 \ll \lambda$) grows linearly with time (see [28]):

$$d = d_0 + t\Delta U_n A(2\pi d_0/\lambda), \tag{13}$$

where $\Delta U_n > 0$ is the change of the normal interface velocity due to the impulse acceleration, $A = |\rho_1 - \rho_2|/(\rho_1 + \rho_2)$ is the Atwood number, ρ_1 and ρ_2 are the densities of the media on both sides of the interface, and the parameters d_0, ρ_1, and ρ_2 are the corresponding values after the impulse acceleration. There is a simple generalization of formula (13) for the case of significant initial disturbances before the stage of turbulent mixing (see [29]).

The other mechanism of the interface instability development in the problem under consideration is the Kelvin–Helmholtz (KH) instability, which occurs when the tangential velocity component becomes discontinuous. The amplitude of the small sinusoidal disturbance of the plane interface, where each medium on different interface sides propagates parallel to the interface with its constant velocity, grows exponentially in time (see [30]):

$$d = d_0 \exp(st), \quad s = (2\pi/\lambda)U_\tau A_K,$$

where $A_K = (\rho_1\rho_2)^{1/2}/(\rho_1 + \rho_2)$ is an analog of the Atwood number and $U_\tau > 0$ is the relative velocity of the media. By restricting ourselves to the consideration of a time interval for which $st \ll 1$, we obtain the formula

$$d = d_0 + tU_\tau A_K(2\pi d_0/\lambda).$$

The rate of growth of the amplitude $\dot{d}$ for both types of instability is

$$\dot{d} = \frac{2\pi d_0}{\lambda}\psi, \tag{14}$$

where $\psi = \Delta U_n A$ for the RM instability and $\psi = U_\tau A_K$ for the KH instability.

Let us return to the two-dimensional problem. On the interface, take a point determined by the given ratio ξ of the distance between this point and the wall to the length of the entire boundary from the wall to the point B (see Fig. 1). In the computation, this implies the choice of a grid interval (since the grid nodes along the interface are placed uniformly). Note that the coordinate z of the point with a given ξ changes only insignificantly with time.

The further analysis is based on the following assumption. The rate of growth of the small interface disturbance in the vicinity of this point is given by formula (14) to a reasonable accuracy, where the parameters d_0 and λ are assumed to be equal for both types of instability, and the parameter ψ is taken from the solution of the two-dimensional problem. The parameter ΔU_n is set to the normal velocity of the chosen interval immediately after the detonation wave has passed (the maximum value of U_n over time was chosen, see Fig. 10). The parameters A and A_K are calculated on the basis of the density values, and the parameter U_τ (the tangential velocity) is calculated on the basis of the velocity component values in the grid cells adjacent to the interval.

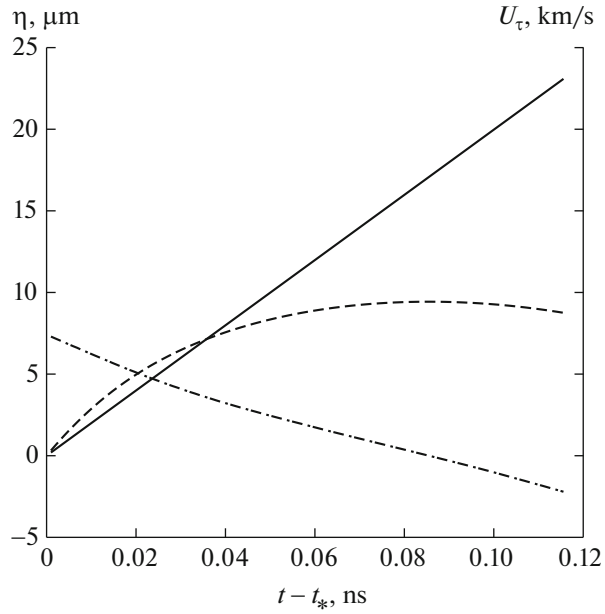

Fig. 11. Time dependence of the function η (15), which is proportional to the difference between the current and initial amplitudes of the small interface disturbance for the Richtmyer–Meshkov (solid curve) and Kevin–Helmholtz (dashed curve) instability and the tangent velocity along the interface (dot-and-dash curve) at the interface point with $z \approx 0.23$ mm.

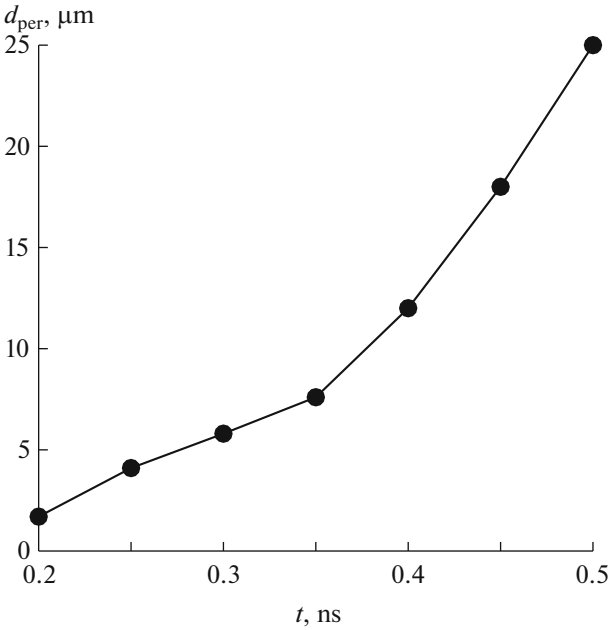

Fig. 12. Amplitude of the local disturbance of the interface as a function of time.

Next, we fix the time t_* at which the detonation wave passes through the chosen interface point (in the computation, we use the time when the maximum of U_n is attained on the chosen grid interval), and calculate the integral

$$\eta(t) = \frac{[d(t) - d_0]\lambda}{2\pi d_0} = \int_{t_*}^{t} \psi(t')dt', \tag{15}$$

Table 2. The velocity $-u_z$ near the local interface disturbance at several time points

t, ns	0.2	0.25	0.3	0.35	0.4	0.45	0.5
$-u_z$, km/s	400	200	0	−300	−600	−1500	−1000

for both types of instability. This integral is proportional to the difference between the current and initial amplitude of the disturbance. Note that, for the RM instability, ψ is independent of time because the impulse acceleration of the interface occurs only at the time when the detonation wave passes (if we restrict ourselves to the time before the reflected wave passage); in the case of the KH instability, the function ψ significantly depends on time because the velocity U_τ is determined by the tangential component of the fuel velocity, which is much greater than the shell velocity and which begins to decrease after the detonation wave passage under the influence of the rarefaction wave.

Figure 11 shows the function $\eta(t - t_*)$ for both types of instability and the function $U_\tau(t - t_*)$ for the point on the interface with $\xi \approx 0.33$ (at the time of the detonation wave front passage, $z \approx 0.23$ mm). The unit vector along the interface on which the velocity vector is projected during the computation of U_τ is oriented in the direction of the detonation wave propagation.

It is seen that first the KH instability gives a faster growth of the amplitude. Then, the velocity U_τ decreases and even changes its sign, which stops the amplitude growth. Hence, we conclude that if formula (14) is valid at least qualitatively, i.e., if the growth rate of the small disturbance amplitude for the KH instability decreases together with the discontinuity of the tangential velocity on the interface, then a noticeable effect of the KH instability on the amplitude growth is possible only at a distance from the detonation wave front, most probably, after the change of the velocity U_τ sign.

Now consider a local disturbance of the interface that occurs during the formation of the detonation wave, which is easily identified at each instant of time and allows us to obtain at least qualitative information about its growth rate. To calculate the local disturbance amplitude at a certain time, we first visually find the extreme nodes that bound the disturbance on the difference grid line that corresponds to the interface. Next, we draw a straight line through these extreme nodes and calculate the maximum positive $d_{\text{per}+}$ and the minimum negative $d_{\text{per}-}$ distances from all interior nodes to this line. The disturbance amplitude is found as $d_{\text{per}} = d_{\text{per}+} - d_{\text{per}-}$.

The found values of the function d_{per} at seven time points are shown in Fig. 12. The values of the velocity $-u_z$ near the local interface disturbance (which are a fairly good approximation of the velocity U_τ considered above) at these time points are shown in Table 2. The decrease of u_z at $t = 0.5$ ns compared with its value at $t = 0.45$ ns is explained by the fact that the reflected detonation wave has not yet reached the interface local disturbance at $t = 0.45$ ns. Recall that the time $t = 0.35$ ns approximately corresponds to the emergence of the reflected detonation wave.

During the time interval between 0.25 and 0.35 ns, the amplitude growth rate dd_{per}/dt is almost invariable even though the sign of the velocity $-u_z$ changes at $t = 0.3$ ns. This suggests the conclusion that the amplitude growth rate before the detonation wave reflection is determined by the RM instability.

It is also seen that the amplitude growth rate for $t > 0.35$ ns is much greater than for $t < 0.35$ ns. The increase in the velocity u_z for $t > 0.35$ ns indicates that the increase in the amplitude growth rate after the detonation wave reflection is caused by the KH instability.

CONCLUSIONS

The ignition of a preliminary compressed DT target with a golden shell by two identical proton beams from its ends is considered. The parameters of the beams ensure the so-called fast ignition with a minimal beam energy. A target of a small size along its axis (the product of initial density by the half-size is approximately 1.3 g/cm^2) is considered.

The reflection of the arising nonstationary spatial detonation wave from the symmetry plane begins near the axis, where a high-pressure region generating a high-speed jet of the DT fuel along the wall in the direction of the boundary with the shell occurs. The formation of the reflected wave completes after this jet hits the shell.

Before the detonation wave is reflected from the symmetry plane, the electron and ion temperature attains its maximum of about 200 MK at a distance from the wave. The maximum photon temperature is about 20 times lower. As the detonation wave is reflected, the maximum ion and electron temperatures rapidly increase by a factor of 2–2.5.

A significant part of the α-particle energy is carried out from the target by flying out particles. During the fuel heating by the proton beam, the fraction of energy loss in unit time is $k_\alpha \approx 0.4$. As the detonation wave propagates, the coefficient k_α gradually decreases to about 0.25–0.3, and after the detonation wave reflection, it rapidly increases due to the increase in the mean free path of the α-particles caused by the decreasing fuel density.

The fuel burn-up factor after the burn stops is $B \approx 0.18$, which is about two times lower than the value obtained in the quasi-one-dimensional model for the same initial fuel density and approximately the same target size. The computation on a coarser grid gives a slightly lower value of B. This allows us to hope that the burn-up factor obtained on a certain grid can be considered as a lower bound on the value of this factor in the exact solution of the problem.

In the region between the wall and the reflected wave, the thermodynamic functions weakly depend on the spatial coordinates, and the velocity component along the axis u_z considered as a function of z has a profile that is close to linear. This allows us to use the known solution to the one-dimensional hydrodynamic equations to approximately describe the dependence of the thermodynamic functions on time by choosing the arbitrary constant in this solution and introducing a correction coefficient based on the results of two-dimensional computations. The burn model thus constructed makes it possible to compute the fuel burn-up factor after the forced termination of the two-dimensional computation due to a high curvature difference grid cells near the curved parts of the fuel-shell interface or due to decreased computation accuracy as the reflected wave goes out of the boundary of the computation domain.

The role of two possible mechanisms of the fuel-shell interface instability development is studied—the impulse acceleration of the interface by the detonation wave (Richtmyer–Meshkov instability) and a high-speed fuel sliding along the interface (Kelvin–Helmholtz instability). The growth of small sinusoidal disturbances of the interface is analyzed on the basis of known formulas for the plane interface; the coefficients in these formulas are taken from computations with the data of the problem under consideration. It is shown that a noticeable influence of the Kelvin–Helmholtz instability on the amplitude growth is possible only at a distance from the detonation wave front, most probably, after the tangent component of the fuel velocity changes its sign due to rarefaction wave adjacent to detonation wave front.

The evolution of a small local disturbance of the interface occurring in the computation of the detonation wave formation is analyzed. The comparison of dependences of the disturbance amplitude and the component u_z of the fuel velocity near the disturbance on time, which may be considered as a jump of the tangent velocity along the interface, suggests the following conclusion, which is close to the conclusion made above as a result of the analysis of small sinusoidal disturbances: the amplitude growth rate before the detonation wave reflection is determined by the Richtmyer–Meshkov instability, and the significant increase in the amplitude growth rate after the reflection is caused by the Kelvin–Helmholtz instability.

REFERENCES

1. E. N. Avrorin, A. A. Bunatyan, A. D. Gadzhiev, et al. "Numerical calculations on fusion detonation in a dense plasma," Sov. J. Plasma Phys. **10** (3), 298–303 (1984).
2. N. G. Basov, S. Yu. Gus'kov, and L. P. Feoktistov, "Thermonuclear gain of ICF targets with direct heating of ignitor," J. Sov. Laser Res. **13** (5), 396–399 (1992). https://doi.org/10.1007/BF01124892
3. M. Tabak, J. Hammer, M. E. Glinsky, et al. "Ignition and high gain with ultrapowerful lasers," Phys. Plasm. **1**, 1626–1634 (1994). https://doi.org/10.1063/1.870664
4. M. M. Basko, M. D. Churazov, and A. G. Aksenov, "Prospects of heavy ion fusion in cylindrical geometry," Laser Part. Beams **20**, 411–414 (2002). https://doi.org/10.1017/S0263034602203080
5. V. V. Vatulin and O. A. Vinokurov, "Fast ignition of the DT fuel in the cylindrical channel by heavy ion beams," Laser Part. Beams **20**, 415–418 (2002). https://doi.org/10.1017/S0263034602203092
6. R. Ramis and J. Meyer-ter-Vehn, "On thermonuclear burn propagation in a pre-compressed cylindrical DT target ignited by a heavy ion beam pulse," Laser Part. Beams **32**, 41–47 (2014). https://doi.org/10.1017/S0263034613000839

7. A. A. Frolova, K. V. Khishchenko, and A. A. Charackhch'yan, "Fast ignition by a proton beam and burning of a DT cylindrical shell target," Plasma Phys. Rep. **45**, 830–649 (2019). https://doi.org/10.1134/S1063780X1908004X
8. K. V. Khishchenko and A. A. Charackhch'yan, "On a property of two symmetrically converging thermonuclear burn plane waves," Vopr. At. Nauki Tekh., Ser. Mat. Modelir. Fiz. Protsessov, No. 3, 30–40 (2013).
9. A. A. Charakhch'yan and K. V. Khishchenko, "Symmetrically converging plane thermonuclear burn waves," Plasma Phys. Control. Fusion. **55**, 105011 (2013). https://doi.org/10.1088/0741-3335/55/10/105011
10. K. V. Khishchenko and A. A. Charackhch'yan, "Collision of plane thermonuclear detonation waves in a preliminarily compressed DT mixture," Plasma Phys. Rep. **41**, 220–230 (2015). https://doi.org/10.1134/S1063780X15020051
11. K. V. Khishchenko and A. A. Charackhch'yan, "On some features of plane waves of thermonuclear burn," J. Appl. Mech. Tech. Phys. **56**, 86–95 (2015). https://doi.org/10.1134/S0021894415010149
12. A. A. Charakhch'yan and K.V. Khishchenko, "Plane thermonuclear detonation waves initiated by proton beams and quasi-one-dimensional model of fast ignition," Laser Part. Beams **33**, 65–80 (2015). https://doi.org/10.1017/S0263034614000780
13. L. I. Sedov, *Similarity and Dimensional Analysis in Mechanics* (Academic, New York, 1959).
14. J. J Duderstadt and G. A. Moses, *Inertial Confinement Fusion* (Wiley, New York, 1982).
15. S. Yu. Gus'kov and V. B. Rozanov, "Kinetics of thermonuclear particles in laser plasma," Tr. Fiz. Inst. Akad. Nauk SSSR **134**, 115–122 (1982).
16. A. A. Charakhch'yan, A. A. Frolova, and K. V. Khishchenko, "The role of heat loss at the fuel-shell interface during the fast ignition of cylindrical DT targets," J. Phys., Conf. Ser. **1147**, 012089 (2019). https://doi.org/10.1088/1742-6596/1147/1/012089
17. K. V. Khishchenko, "Equations of state for two alkali metals at high temperatures," J. Phys., Conf. Ser. **98**, 032023 (2008). https://doi.org/10.1088/1742-6596/98/3/032023
18. W. B. Holzapfel, "Equation of state for Cu, Ag, and Au and problems with shock wave reduced isotherms," High Pressure Res. **30**, 372–394 (2010). https://doi.org/10.1080/08957959.2010.494845
19. A. G. Kulikovsii, N. V. Pogorelov, and A. Yu. Semenov, *Mathematical Issues of Numerical Solution of Hyperbolic Systems of Equations* (Fizmatlit, Moscow, 2001) [in Russian].
20. A. A. Frolova, K. V. Khishchenko, and A. A. Charackhch'yan, "Track method for the calculation of plasma heating by charged thermonuclear reaction products for axisymmetric flows," Comput. Math. Math. Phys. **56**, 437–449 (2016). https://doi.org/10.1134/S0965542516030052
21. A. A. Charackhch'yan, "Calculation of the compression of deuterium in a conical target in the framework of the Navier–Stokes equations for two-temperature magnetohydrodynamics," Comput. Math. Math. Phys. **33** (5), 683–697 (1993).
22. V. V. Milyavskii, V. E. Fortov, A. A. Frolova, K. V. Khishchenko, A. A. Charakhch'yan, and L. V. Shurshalov, "Calculation of shock compression of porous media in conical solid-state targets with an outlet hole," Comput. Math. Math. Phys. **46**, 873–890 (2006). https://doi.org/10.1134/S0965542506050113
23. S. A. Ivanenko and A. A. Charackhch'yan, "An algorithm for constructing curvilinear grids consisting of convex quadrangles," Soviet Math. Dokl. **36** (1), 51–54 (1988).
24. S. A. Ivanenko and A. A. Charackhch'yan, "Curvilinear grids of convex quadrangles," USSR Comput. Math. Math. Phys. **28** (2), 126–133 (1988).
25. A. A. Charackhch'yan and S. A. Ivanenko, "A variational form of the Winslow grid generator," J. Comput. Phys. **136**, 385–398 (1997). https://doi.org/10.1006/jcph.1997.5750
26. V. I. Gryn', A. A. Frolova, and A. A. Charackhch'yan, "A barrier-type grid generator and its application in flow computations with moving boundaries," Comput. Math. Math. Phys. **43**, 863–869 (2003).
27. L. D. Landau and E. M. Lifshitz, *Fluid Mechanics*, 2nd ed. (Pergamon, Oxford, 1987).
28. R. D. Richtmyer, "Taylor instability in shock acceleration of compressible fluids," Commun. Pure Appl. Math. **13**, 297–319 (1960). https://doi.org/10.1002/cpa.3160130207
29. A. A. Charakhch'yan, "Reshocking at the non-linear stage of Richtmyer–Meshkov instability," Plasma Phys. Controlled Fusion **43**, 1169–1179 (2001). https://doi.org/10.1088/0741-3335/43/9/301
30. P. G. Drazin, *Introduction to Hydrodynamic Stability* (Cambridge Univ. Press, Cambridge, 2002).

Translated by A. Klimontovich